Intensity-symmetric Airy beams

P. Vaveliuk,[1,2,*] Alberto Lencina,[1,3] Jose A. Rodrigo,[4] and Ó. Martnez-Matos[4]

[1]*Centro de Investigaciones Ópticas (CONICET La Plata–CIC), Cno. Centenario y 506, P.O. Box 3, 1897 Gonnet, Argentina*
[2]*Facultade de Tecnologia, Servicio Nacional de Aprendizagen Industrial SENAI-Cimatec, Av. Orlando Gomes 1845 41650-010, Salvador, Bahia, Brazil*
[3]*Departamento de Física, Fac. de Cs. Exactas, Universidad Nacional de La Plata, P.O. Box 67, 1900 La Plata, Argentina*
[4]*Universidad Complutense de Madrid, Facultad de Ciencias Fsicas, Ciudad Universitaria s/n, Madrid 28040, Spain*
**Corresponding author: pvaveliu@fis.ucm.es*

Received November 11, 2014; accepted January 9, 2015;
posted January 22, 2015 (Doc. ID 226603); published February 16, 2015

Theoretical, numerical, and experimental research on a novel family of Airy beams in rectangular coordinates having a symmetric transverse pattern of light intensity is presented. The intensity-symmetric Airy beams include both the symmetric Airy beam whose field amplitude is an even function of the transverse coordinates and the antisymmetric Airy beam whose field amplitude is an odd function of such coordinates. The theoretical foundations are based on the relationship of the symmetries of the spectral phase with the cosine and sine Fourier transforms. These beams are analyzed in a propagation range also including the region preceding the Fourier plane. These beams exhibit autofocusing, collapse, self-bending, and reversal propagation. Moreover, the intensity distribution is strongly asymmetric with respect to the Fourier plane. All these peculiar features were not reported for other classes of paraxial beams in a rectangular frame. The experimental generation of intensity-symmetric Airy beams is demonstrated supporting the theoretical predictions. Possible applications in planar waveguide writing and optical trapping are also discussed.

OCIS codes: (140.3300) Laser beam shaping; (260.0260) Physical optics; (070.2580) Paraxial wave optics; (350.5500) Propagation.
http://dx.doi.org/10.1364/JOSAA.32.000443

1. INTRODUCTION

The watermark of the accelerating Airy beam (AiB) is undoubtedly its spectral cubic phase modulated by a Gaussian amplitude [1,2]. This peculiar phase governs its self-bending characteristic in propagation. Several experimental techniques for the generation of Airy beams have been reported elsewhere [2–5]. In particular, the AiB can be generated at the focal plane of a lens by Fourier transforming its angular spectrum [2]. In this context, the manipulation of the AiB angular spectrum allowed us to recently introduce a new kind of Airy beam referred to as the symmetric Airy beam (SAB) [6]. This beam arises from the conventional Airy beam by changing the parity of the spectral cubic phase: an odd parity by an even one. This change brings deep differences in the propagation dynamics of both beams. The SAB presents autofocusing and collapse during propagation. Up to that time, these properties were entirely associated with Airy beams having cylindrical symmetry [7–9]. Moreover, the intensity pattern results are symmetric in the transverse spatial coordinates because the angular spectrum presents an even parity in the transverse spatial frequency. Considering that the Fourier transform of an even function can be regarded as a cosine Fourier transform, the SAB results are symmetric in its field amplitude as well. However, the SAB does not constitute the unique intensity-symmetric Airy beam (ISAB) since it is feasible to obtain an ISAB possessing an antisymmetric field amplitude. The Fourier transform properties of parity-defined functions permit an odd extension of the angular spectrum allowing the generation of an intensity-symmetric beam from an antisymmetric field amplitude. These beams are represented by a sine Fourier transform leading us to introduce the *antisymmetric Airy beam* (ASAB) from the odd extension of the AiB spectrum.

In this paper we present a theoretical, numerical, and experimental study encompassing the ISABs, including the region preceding the Fourier plane, which was not previously addressed [6]. This full analysis emphasizes the main propagation properties. Finally, we discuss the potential applications of ISABs.

2. THEORETICAL FRAMEWORK

We start from the theoretical analysis [10] of the intensity-symmetric Airy beams within the angular spectrum representation [6,11]. The paraxial field solution for a SAB, $v(\cdot)$, propagating in the $\tilde{z}$ direction was expressed in [6] as

$$v_{\pm}(\tilde{x},\tilde{z}) = \frac{1}{2\pi}\int_{-\infty}^{+\infty} \mathrm{d}\tilde{K} V_{\pm}^{e}(\tilde{K}) e^{i2\pi\tilde{z}[1-\tilde{K}^2/(8\pi^2)]} e^{i\tilde{K}\tilde{x}}, \tag{1}$$

where $V_{\pm}^{e}(\tilde{K}) \equiv \mathcal{F}\{v_{\pm}(\tilde{x},0)\}$ is the FT of $v_{\pm}(\tilde{x},\tilde{z})$ at the lens Fourier plane $\tilde{z}=0$ and the superscript e refers to an even extension of the AiB angular spectrum. Explicitly,

$$V_{\pm}^{e}(\tilde{K}) = Ce^{-a\tilde{K}^2\tilde{x}_0^2} e^{\pm i|\tilde{K}|^3\tilde{x}_0^3/3} \tag{2}$$

includes the Gaussian amplitude and the cubic phase with even parity. The constant $C=\tilde{x}_0\exp(a^3/3)$ is the amplitude of the angular spectrum. The above equations are expressed using dimensionless variables: the propagation variable, $\tilde{z}=z/\lambda$; the transverse spatial variable, $\tilde{x}=x/\lambda$; and the

conjugate variable, $\tilde{K} = \lambda K$, λ being the wavelength. As in the case of conventional Airy beams, the parameter x_0 (or its associated dimensionless parameter $\tilde{x}_0 = x_0/\lambda$) refers to the beam transverse size, and the parameter $a > 0$ guarantees the square integrability of the solution [1,12]. Based on the FT properties of even functions [13], the field $v_\pm$ results in an even function of transverse spatial variable $\tilde{x}$, i.e., $v_\pm^e \equiv v_\pm$. It can be expressed by means of a Fourier cosine transform:

$$v_\pm^e(\tilde{x},\tilde{z}) = \frac{1}{\pi} \times \int_0^\infty d\tilde{K} V_\pm(\tilde{K}) e^{i2\pi\tilde{z}[1-\tilde{K}^2/(8\pi^2)]} \cos(\tilde{K}\tilde{x}), \quad (3)$$

where $V_\pm(\tilde{K})$ is the part of $V_\pm^e(\tilde{K})$ corresponding to $K > 0$. Then, as a result of an even extension of the AiB angular spectrum, the SAB is symmetric in field amplitude and in intensity distribution. On the other hand, the odd extension of $V_\pm(\tilde{K})$ to the overall $\tilde{K}$-range, namely, $V_\pm^o(\tilde{K})$, leads to a beam whose field amplitude, $v^o(\cdot)$, is an antisymmetric function of $\tilde{x}$. Explicitly,

$$v_\pm^o(\tilde{x},\tilde{z}) = \frac{1}{2\pi} \int_{-\infty}^{+\infty} d\tilde{K} V_\pm^o(\tilde{K}) e^{i2\pi\tilde{z}[1-\tilde{K}^2/(8\pi^2)]} e^{i\tilde{K}\tilde{x}} \quad (4)$$

so that the odd angular spectrum

$$V_\pm^o(\tilde{K}) = \mathrm{sgn}(\tilde{K}) V_\pm^e(\tilde{K}) \quad (5)$$

has an even cubic phase with a π-discontinuity (dislocation) at $\tilde{K} = 0$ as a consequence of the antisymmetrization. sgn represents the sign function in Eq. (5). The field amplitude of this *antisymmetric Airy beam* (ASAB) can be expressed by a Fourier sine transform,

$$v_\pm^o(\tilde{x},\tilde{z}) = \frac{i}{\pi} \times \int_0^\infty d\tilde{K} V_\pm(\tilde{K}) e^{i2\pi\tilde{z}[1-\tilde{K}^2/(8\pi^2)]} \sin(\tilde{K}\tilde{x}), \quad (6)$$

in analogy with the SAB expressed by Eq. (3).

3. SIMULATED RESULTS

Equations (1)–(6) encompass the theoretical model of ISABs. Notice that there exist two solutions for SABs (v_+^e, v_-^e) [Eqs. (1)–(3)] and two solutions for ASABs (v_+^o, v_-^o) [Eqs. (4)–(6)]. This fact is due to the conjugate phases in their respective angular spectra [Eqs. (2) and (5)]. Figure 1 shows the intensity distributions for SABs, Fig. 1(a) $|v_+^e|^2$ and Fig. 1(b) $|v_-^e|^2$; and for ASABs, Fig. 1(c) $|v_+^o|^2$ and Fig. 1(d) $|v_-^o|^2$, as a function of $s = \tilde{x}/\tilde{x}_0$ and $\xi = \tilde{z}/(2\pi\tilde{x}_0^2)$ for the overall propagation range, including the region before the Fourier plane. These results indicate that ISABs are not symmetric in the intensity distribution with respect to the Fourier plane $\xi = 0$ or to any other transverse plane including the autofocusing plane. Besides, $v_+^{e,o}$ (*direct propagation*) and $v_-^{e,o}$ (*inverse propagation*) have inverted propagation dynamics. It is worth noting that either can easily be generated by modulating an input Gaussian beam with a proper phase function encoded into a spatial light modulator. We recall that a conventional AiB is also invertible. Nevertheless, its intensity distribution exhibits symmetry along the axial coordinate from the plane $\xi = 0$ so that there are no different propagation dynamics arising from conjugate phase masks. In contrast, conjugate masks only generate AiB with an opposite bending direction.

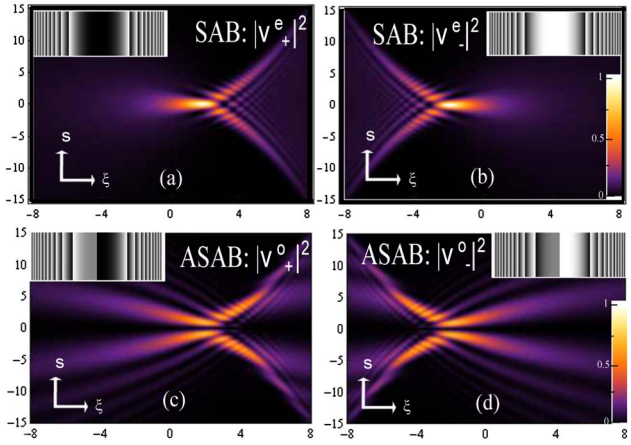

Fig. 1. Theoretical intensity distributions for ISABs as a function of (s,ξ). (a) and (b) SABs generated from conjugated spectral phases. (c) and (d) Idem for ASABs. The insets show the phase masks wrapped between 0 (black) and 2π (white). The intensity scale is normalized to the maximum intensity for the SAB pattern. The beam parameters are $\tilde{x}_0 = 100$ and $a = 0.08$.

Figure 1 supports that an ISAB has unique properties in rectangular coordinates: it exhibits a relevant asymmetry along the propagation coordinate, autofocusing, collapse, and self-bending. However, there are differences in the propagation dynamics of SABs and ASABs fundamentally based on a different interference process for both beams due to different symmetry in their respective electric fields. If E_+ is the field due to the contribution from all points $x > 0$, the total field for the SAB is $(E_+ + E_-)$ because the even parity. In turn, if E_- is the field due to the contribution from all points $x < 0$, the total field for the ASAB is $(E_+ - E_-)$ because of the odd parity. This leads the SAB to exhibit better focusing ability due to efficient constructive interference. The SAB focuses in a single focus of $\Delta s_{\mathrm{SAB}} = 1.3$ at FWHM which contains 73% of the energy of the beam, while for ASAB, the beam has no central focusing lobe due to a zero on-axis intensity in the overall propagation range. Instead of this, 64% of the beam energy is contained in two principal specularly symmetric off-axis lobes of $\Delta s_{\mathrm{ASAB}} = 1.15$ at FWHM for each one. The lobe separation size is about 0.8.

Figure 2 shows numerical simulations of 2D transverse profiles as a function of transverse spatial coordinates (s_x, s_y) on the direct propagation scheme. The intensity distribution for SABs and ASABs at planes $\xi = -\xi_f$, 0, ξ_f, $1.5\xi_f$, $2\xi_f$ are displayed in the first and second row of Fig. 2. The autofocusing plane is located at $\xi_f = 1.9$ (as in the 1D case) for both classes of beams. The intensity distribution is nonsymmetric with respect to $\xi = \xi_f$. This plane divides two quite different propagation regions. Specifically, for $\xi \le \xi_f$, ISABs autofocus into a shape-preserving fashion, while for $\xi > \xi_f$, ISABs defocus in a nonpreserving shape-forming self-bending lobe. After the autofocusing plane $\xi = \xi_f$, the intensity has a square-like shape distribution and tends to mostly concentrate in the vertices. However, there is a significant difference between SABs and ASABs arising from the edge dislocations present in the phase of the later beam as a consequence of the antisymmetry in its angular spectrum. This fact forces the ASAB to have zero intensity at $s_x = s_y = 0$, redistributing a higher intensity concentration to the vertices.

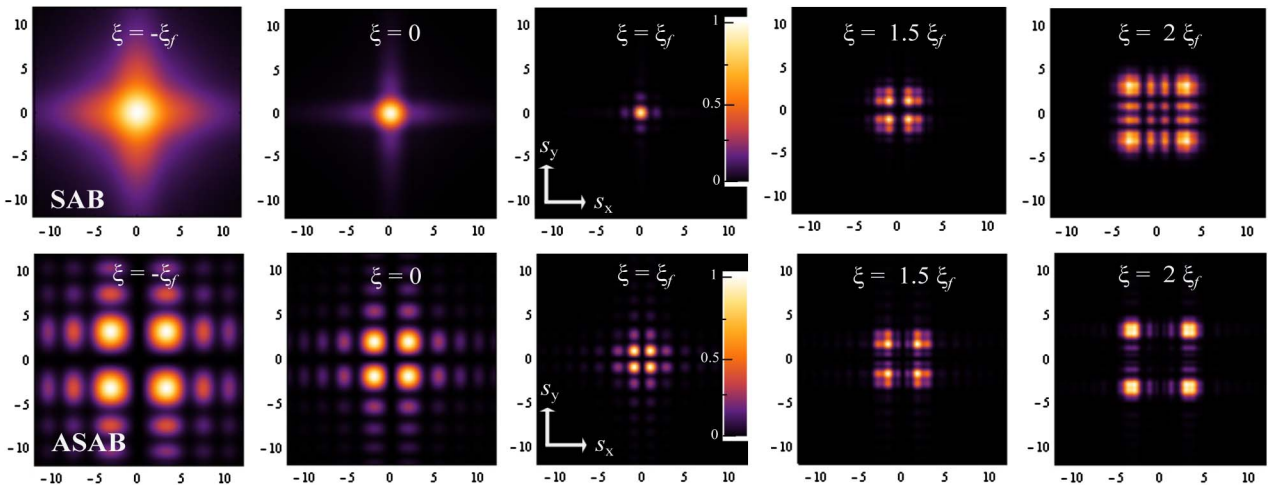

Fig. 2. Theoretical intensity patterns for a SAB (first row) and for an ASAB (second row) as a function of transverse coordinates (s_x, s_y) for several planes $\xi = -\xi_f$, 0, ξ_f, $1.5\xi_f$, $2\xi_f$, where ξ_f is the distance between the Fourier and autofocusing planes. The intensity scale is normalized to the maximum intensity for each snapshot.

Let us now study the autofocusing property of ISABs. We emphasize that no other kinds of beams were analyzed possessing autofocusing in a rectangular frame, neither theoretical nor experimental. In free propagation, the energy flux tends to suddenly accumulate into a small area at the autofocus, such that the intensity peak at this region can reach up several orders of magnitude of the input peak intensity. Figure 3 depicts the peak intensity normalized to the peak intensity at the plane $\xi = -8$ for a SAB [Fig. 3(a)] and for an ASAB [Fig. 3(b)] in the overall propagation range. For the SAB, the normalized peak intensity at the autofocus ($\xi = \xi_f = 1.9$) reaches ≈570, although there are autofocusing waves (which, however, are not Airy functions) reaching a peak contrast of ∼10, 000 in cylindrical coordinates [8]. We believe that the high contrast, as well as the collapse, achieved by the SAB is related to a cusp caustic field structure [14]. Thereby, the intensity contrast can be as high as for circular symmetric Airy beams. On the other hand, the peak intensity contrast between the autofocus and the input plane for the ASAB is ≈65, as Fig. 3(b) shows. Therefore, the autofocusing property of the ASAB is much weaker than for SAB. In contrast, the ASAB beam energy is not mostly concentrated in a small size around the autofocus but it is extended in a wide propagation interval. For instance, the normalized peak intensity varies between 40 and 60 in the range $\xi \approx 3$ up to $\xi \approx 5$. Taking into account these properties, the SABs could be used in applications where a high intensity contrast is needed in propagation. In this context, the SABs have recently been used as an optical trap [15]. On the other hand, the geometry of ASABs could be exploited in photonic applications such as planar waveguide writing, where it is required that the beam energy should be distributed in a broader propagation range [16]. The fluctuations in the intensity along the propagation direction do not affect the writing process predominantly since the waveguide writing is performed in the transverse direction.

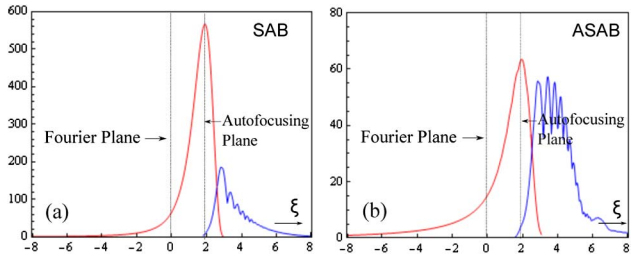

Fig. 3. Peak intensity normalized to the peak intensity at the initial plane as a function of ξ for (a) SAB and (b) ASAB in the direct propagation scheme. For the SAB, the red line corresponds to the central lobe, while for the ASAB it corresponds to the two main lobes collapsing at $\xi \approx 3$. The blue lines correspond to the main curved lobes arising shortly before the collapse. The initial propagation plane is taken at $\xi = -8$.

4. EXPERIMENTAL RESULTS

Finally, the experimental generation of ISABs is demonstrated considering a similar optical implementation as reported in [6]. In this case, we include the overall propagation range including the negative values of ξ. The beam's complex field amplitude was encoded as a phase-only computer-generated hologram (CGH) following the approach reported in [17]. In our case, the CGH was addressed into a programmable reflective LCoS-SLM (Holoeye PLUTO, 8-bit gray-level, pixel pitch of 8 μm, and 1920 × 1080 pixels) calibrated for a 2π phase shift at the wavelength $\lambda = 532$ nm and corrected from static aberrations as reported in [18]. To generate the Airy beams, the hologram was illuminated by a collimated laser beam ($\lambda = 532$ nm) and then focused by a spherical convergent lens (focal length of 10 cm, N-BK7 glass). The beam propagation has been measured around the focal plane by using a CCD camera (Spiricon SP620U, 12-bit gray-level, pixel pitch of 4.4 μm). Figure 4 shows 2D transverse profiles of the direct propagation scheme obtained from the experiments. The intensity distribution for SABs and ASABs at planes $z = -z_f$, 0, z_f, $1.5z_f$, $2z_f$, with $z_f = 5.7$ mm being the distance between the Fourier and the autofocusing planes, are displayed in the first and second row of Fig. 4. These results are in good agreement with the theoretical expectation displayed in Fig. 2. We also verify (not shown) that the conjugate phase mask inverts the propagation dynamics of the beam as was predicted in the theoretical context validating the ISABs propagation features.

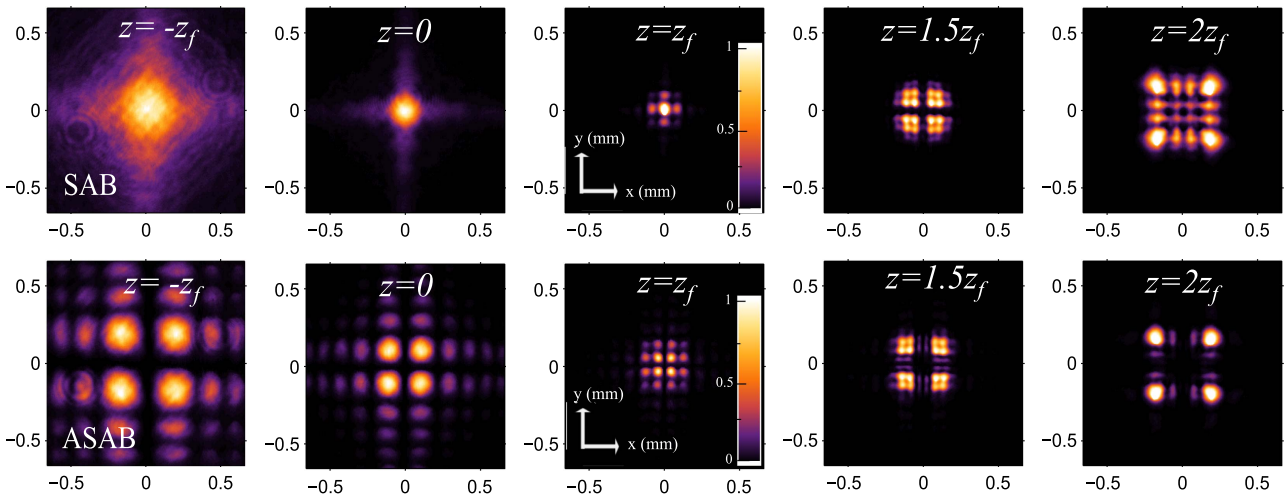

Fig. 4. Experimental intensity patterns for a SAB (first row) and for an ASAB (second row) as a function of (x, y) for several planes $z = -z_f$, 0, z_f, $1.5z_f$, $2z_f$, with $z_f = 5.7$ mm being the distance between the Fourier and autofocusing planes. The intensity scale is normalized to the maximum intensity for each snapshot.

5. CONCLUSIONS

In conclusion, full theoretical, numerical, and experimental research on intensity-symmetric Airy beams was performed. Their propagation characteristics have been presented in detail. The theoretical foundations were based on the relationship of the symmetries of the spectral phase with the cosine and sine Fourier transforms. These beams were analyzed in a propagation range also including the region preceding the Fourier plane. Intensity-symmetric Airy beams exhibit autofocusing, collapse, self-bending, and reversal propagation. These features have not been reported in other classes of paraxial beams in a rectangular frame. From the analysis, it was established that the SAB exhibits a better focus capability than the ASAB. Nevertheless, the ASAB keeps its intensity shape over a wider propagation range. These features make them complementary for optical applications.

ACKNOWLEDGMENTS

The project TEC 2011-23629 (Spain) and CNPq (Brazil) are acknowledged.

REFERENCES AND NOTES

1. G. A. Siviloglou and D. N. Christodoulides, "Accelerating finite energy Airy beams," Opt. Lett. **32**, 979–981 (2007).
2. G. A. Siviloglou, J. Broky, A. Dogariu, and D. N. Christodoulides, "Observation of accelerating Airy beams," Phys. Rev. Lett. **99**, 213901 (2007).
3. J. A. Davis, M. J. Mitry, M. A. Bandres, I. Ruiz, K. P. McAuley, and D. M. Cottrell, "Generation of accelerating Airy and accelerating parabolic beams using phase-only patterns," Appl. Opt. **48**, 3170–3176 (2009).
4. D. M. Cottrell, J. A. Davis, and T. M. Hazard, "Direct generation of accelerating Airy beams using a 3/2 phase-only pattern," Opt. Lett. **34**, 2634–2636 (2009).
5. D. G. Papazoglou, S. Suntsov, D. Abdollahpour, and S. Tzortzakis, "Tunable intense Airy beams and tailored femtosecond laser filaments," Phys. Rev. A **81**, 061807 (2010).
6. P. Vaveliuk, A. Lencina, J. A. Rodrigo, and O. Martinez Matos, "Symmetric Airy beams," Opt. Lett. **39**, 2370–2373 (2014).
7. N. K. Efremidis and D. N. Christodoulides, "Abruptly autofocusing waves," Opt. Lett. **35**, 4045–4047 (2010).
8. I. D. Chremmos, N. K. Efremidis, and D. N. Christodoulides, "Pre-engineered abruptly autofocusing beams," Opt. Lett. **36**, 1890–1892 (2011).
9. D. G. Papazoglou, N. K. Efremidis, D. N. Christodoulides, and S. Tzortzakis, "Observation of abruptly autofocusing waves," Opt. Lett. **36**, 1842–1844 (2011).
10. The theoretical background is developed here for one transverse dimension. The extension to 2D is direct.
11. P. Vaveliuk and O. Martinez Matos, "Negative propagation effect in nonparaxial Airy beams," Opt. Express **20**, 26913–26921 (2012).
12. I. M. Besieris and A. M. Shaarawi, "A note on an accelerating finite energy Airy beam," Opt. Lett. **32**, 2447–2449 (2007).
13. P. Yip, "Sine and cosine transforms," in *The Transforms and Applications Handbook*, A. D. Poularikas, ed., 2nd ed. (CRC Press, 2000), Chap. 3.
14. Y. A. Kravtsov and Y. I. Orlov, *Caustics, Catastrophes and Wave Fields*, 2nd ed. (Springer-Verlag, 1999).
15. P. A. Quinto-Su and R. Juregui, "Optical stacking of microparticles in a pyramidal structure created with a symmetric cubic phase," Opt. Express **22**, 12283–12288 (2014).
16. D. Biasetti, E. Neyra, J. R. Vzquez de Aldana, L. Roso, and G. A. Torchia, "Buried waveguides in Nd:YLF crystals obtained by femtosecond laser writing under double line approach," Appl. Phys. A **110**, 595–599 (2013).
17. J. A. Davis, D. M. Cottrell, J. Campos, M. J. Yzuel, and I. Moreno, "Encoding amplitude information onto phase-only filters," Appl. Opt. **38**, 5004–5013 (1999).
18. J. A. Rodrigo, T. Alieva, A. Cámara, O. Martínez-Matos, P. Cheben, and M. L. Calvo, "Characterization of holographically generated beams via phase retrieval based on Wigner distribution projections," Opt. Express **19**, 6064–6077 (2011).